Intestinal barrier function in the naked mole-rat: an emergent model for gastrointestinal insights

Javier Aguilera-Lizarraga[1]*, Anne Ritoux[1], David C. Bulmer[1], Ewan St. John Smith[1]*

[1] Department of Pharmacology, University of Cambridge, Cambridge, United Kingdom

* To whom correspondence should be addressed: Dr. Javier Aguilera-Lizarraga: ja783@cam.ac.uk; Prof. Ewan St. John Smith: es336@cam.ac.uk.

Abstract:

The intestinal barrier plays a crucial role in homeostasis, both by facilitating absorption of nutrients and providing a tight shield to prevent the invasion by either pathogen or commensal microorganisms. Intestinal barrier malfunction is associated with systemic inflammation, oxidative stress, and decreased insulin sensitivity, which may lead to the dysregulation of other tissues such as the liver, fat, skeletal muscle, and brain. Hence, a deeper understanding of physiological aspects related to an enhanced barrier function is of great clinical relevance. The naked mole-rat (*Heterocephalus glaber*) has many unusual biological features, including impaired colonic neuron sensitivity to acid and bradykinin, and resistance to chemically induced intestinal damage. However, insight into their intestinal barrier physiology is scarce. Here, we observed notable differences in intestinal tissue structure between naked mole-rats and mice, especially in the ileum. This was characterised by thicker muscularis and submucosa layers, longer villi and larger crypts. In measuring gut permeability, naked mole-rats showed reduced permeability compared to mice, especially in the small intestine (ileum). Furthermore, intestinal anion secretion induced by serotonin, bradykinin, histamine and capsaicin was significantly impaired in naked mole-rats compared to mice, despite the expression of receptors for all these agonists. Collectively, these findings indicate that naked mole-rats possess a robust gastrointestinal barrier, that is hard to penetrate and is resistant to environmental and endogenous irritants. Naked mole-rats may therefore provide valuable insights into the physiology of the intestinal barrier related to different pathological conditions and set the stage for the development of innovative and effective therapies.

Keywords: gut; intestinal function; naked mole-rat; intestinal permeability; mucosal anion secretion;

1. Introduction:

Digestive pathologies stand out as the most common type of disease worldwide (*1*). Importantly, they result in a significant reduction in the quality of life for patients and represent a multi-billion healthcare burden globally (*2–5*). Intestinal barrier dysfunction is a common feature of most gastrointestinal diseases, including coeliac disease, inflammatory bowel disease, metabolic dysfunction-associated liver disease and disorders of gut-brain interaction (*6*). Moreover, numerous pathologies unrelated to the gastrointestinal tract, such as respiratory diseases (*7*), skin conditions (*8*) and neurodegenerative diseases (*9*), have also been associated with impaired intestinal barrier function. The common denominator of intestinal barrier perturbation led to the "leaky gut" hypothesis (*10*), which states that enhanced intestinal permeability, caused by endogenous or exogenous factors, may increase the passage of food antigens, commensal microorganisms and/or pathogens into the underlying tissue and the systemic circulation, leading to aberrant immune activation described in different disease conditions. Although increased permeability may not necessarily be deleterious (*11*), and whether intestinal barrier dysregulation is the cause or consequence in most disorders is unknown, it is broadly accepted that adequate functioning of the intestinal barrier is required to maintain gut and inter-organ homeostasis. Consequently, identifying mechanisms leading to enhanced intestinal barrier function is highly relevant for both basic and clinical sciences.

In addition to the use of human intestinal mucosal biopsies (*12*), many models have been employed to investigate the (patho)physiology of the intestinal barrier. Among these, gut-derived cell lines (*13*), such as Caco-2 cell monolayers (*14*), and animal models, primarily rodents, but also porcine, equine and avian models (*15*), have been most commonly utilised. Furthermore, human organoids have recently been implemented to model intestinal epithelial barrier function (*16, 17*). Despite important advances in our understanding of intestinal barrier function, there has been little to no reduction in the global incidence and prevalence of gastrointestinal conditions over the last 30+ years (*1*). There is thus an imperative need for further research, including the development of novel models, to enhance understanding of intestinal barrier function.

In recent years, naked mole-rats (NMRs, *Heterocephalus glaber*) have attracted considerable attention from scientists as a non-traditional animal model due to their highly unusual biological features (*18*). Notably, these animals show an outstanding tolerance to environmental stressors associated with human diseases. Indeed, these eusocial rodents, which have an unusually long lifespan (>35 years) (*19*), have been used for investigating 'healthy' aging (*20*), cancer resistance (*21*), and protection against neurodegeneration (*22*). However, the gastrointestinal tract of these animals remains poorly characterised. Of interest, a recent study revealed that the intestinal barrier of NMRs is resistant to tissue damage induced by dextran sodium sulphate (DSS) (*23*), a widely used colitogenic chemical for modelling inflammatory bowel disease. Although the authors employed a modified version of the traditional DSS protocols (*24*), NMRs displayed no signs of histological damage, even when exposed to 8.75% DSS, albeit for only 3-days. We therefore hypothesised that NMRs would display enhanced intestinal function, that is, improved permeability and resistance to intestinal irritants. To answer this question, we explored the macroscopic and microscopic features of the NMR gut, intestinal permeability, changes in mucosal anion secretion, and expression of intestinal

markers of biological interest. Investigating the intestinal barrier function in NMRs may enable a better understanding of the underlying mechanisms that contribute to better mucosal protection.

2. Material and Methods:

2.1. Animals

All animal experiments were performed in accordance with the Animals (Scientific Procedures) Act 1986 Amendment Regulations 2012 under Project Licenses granted to E.St.J.S. (P7EBFC1B1 and PP5814995) by the Home Office and approved by the University of Cambridge Animal Welfare Ethical Review Body. Experiments were performed using a mixture of male and female C57BL6/J mice (10-15 weeks old; IQR 10-12) and a mixture of male and female, non-breeder, NMRs (23-145 weeks; IQR 48-54). Mice were purchased from Envigo and housed conventionally with nesting material and a red plastic shelter in a temperature-controlled room at 21 °C, with a 12-hour light/dark cycle and access to food and water *ad libitum*. NMRs were bred in-house and maintained in an interconnected network of cages in a humidified (~55%) temperature-controlled room at 28-32 °C with red lighting (08:00−16:00). NMRs had access to food *ad libitum*. In addition, a heat cable provided extra warmth under two to three cages/colony. NMRs used in this study came from five different colonies. Animals were humanely killed by CO_2 exposure followed by cervical dislocation (mice) or decapitation (NMRs).

2.2. Intestinal tissue processing for histology and histomorphometric assessment

Intestinal biopsies (ileum and colon) were fixed and embedded using conventional techniques. In brief, samples were incubated, after dissection, in 4% paraformaldehyde (PFA) at 4 °C overnight. Next, samples were washed in PBS, transferred to sucrose (0.3 g · ml^{-1}) and stored at 4 °C overnight. Finally, samples were embedded in Shandon M-1 Embedding Matrix (Thermo Fisher Scientific), snap-frozen and stored at −80°C until processing. Cryostat (Leica) sections (12 µm) were collated across Superfrost Plus slides (Thermo Fisher Scientific) and stained with haematoxylin and eosin (H&E) using conventional techniques (*25, 26*). The number of villi (in ileum samples), number of crypts, villi length and width, crypt length and width, and thickness of the different layers (submucosa and muscularis) were measured in ileum and colon samples using ImageJ software. For analyses of villi and crypts, only intestinal units that were apparently complete and full-sized, and showed no signs of bending or mechanical damage, were chosen in each sample. A total of 5-10 units of each kind were carefully selected, and their average calculated.

2.3. Ussing chambers

Post-mortem, for both species, the gastrointestinal tract (from pyloric sphincter to anus) was carefully removed, cleaned of faecal pellets and maintained in ice-cold Krebs solution. For experiments where transepithelial electrical resistance (*TEER*) was measured, full-thickness segments of ileum and colon were mounted in Ussing chambers without removal of the muscularis propria or the serosa. For experiments where short-circuit current (I_{sc}) was measured, ileum samples were pinned in Sylgard plates with the lamina propria facing down

121 and muscularis externa and serosal layers gently peeled off with forceps to prepare lamina
122 propria-submucosal plexus intestinal strips. Multichannel DVC 1000 Voltage/Current clamp
123 apparatus (World Precision Instruments) was used to measure changes in intestinal tissue
124 function. Each channel was connected to a DVC-3 preamplifier (World Precision Instruments),
125 connected to two current and two voltage electrodes filled with 1.5% (w/v) agar (Millipore)
126 dissolved in 3M KCl. The voltage and fluid resistance were zeroed to eliminate electrical bias
127 and the voltage clamp circuitry was set to standby mode and the intestinal preparation was
128 mounted in the chamber with fresh superfusate. After calibration, intestinal tissues were then
129 mounted in Ussing chambers and the mucosal and serosal compartments were bathed
130 independently with 10 mL of Krebs-Ringer bicarbonate buffer (pH 7.4) containing (in mM): 118
131 NaCl; 4.7 KCl; 1.2 $CaCl_2$; 1.2 $MgSO_4$; 1.2 NaH_2PO_4; 25 $NaHCO_3$). Glucose (10 mM) was
132 present in the medium that bathed the serosal surface of the tissue and mannitol (10 mM) was
133 substituted for glucose in the medium that bathed the mucosal surface. Media were
134 oxygenated (95% O_2, 5% CO_2) throughout the experiment via a gas-uplift recirculation system
135 and maintained at 37˚C by water-jacketed reservoirs. Although NMRs are cold blooded and
136 maintained at 28-32 °C, to minimise the number of variables impacting our results, all
137 experiments were conducted with media maintained at 37 °C. For mouse tissue, Ussing
138 chambers with an exposed area of 0.071 cm^2 were used, while an exposed area of 0.196 cm^2
139 was used for NMR tissue.

140 *Transepithelial electrical resistance (TEER) experiments*: The transepithelial electrical
141 resistance was calculated according to Ohm's law (resistance = voltage/current, normalised
142 by the exposed window area; TEER = $R_{tissue}(\Omega) \cdot$ Area (cm^2)) from the voltage deflections
143 induced by bipolar current pulses of 50 µA every 50 s with a duration of 500 ms). After 30 min
144 of tissue stabilisation, TEER was measured over a period of 2 h.

145 *Short-circuit current* (I_{sc}) *experiments*: After mounting, tissue was allowed to equilibrate for 15-
146 20 min. Thereafter, preparations were short-circuited (voltage-clamped at zero potential) and
147 the short-circuit current (I_{sc}) required to maintain the 0 mV potential was monitored over time.
148 After short-circuiting, intestinal tissue allowed to equilibrate for 10-15 min to allow bioelectric
149 measures to stabilise (baseline). All I_{sc} responses were normalised to µA · cm^{-2} and changes
150 in I_{sc} (ΔI_{sc}) were recorded after application of compounds to the serosal side.

151

152 ***2.4. Chemicals***

153 The following drugs were used for short-circuit current (I_{sc}) experiments: capsaicin (Sigma-
154 Aldrich), bradykinin (Tocris), 5-hydroxytryptamine (5-HT, serotonin) (Sigma-Aldrich) and
155 histamine (Sigma-Aldrich). Capsaicin (1 mM) was dissolved in 100% ethanol and bradykinin
156 (1 mM), 5-HT (10 mM) and histamine (10 mM) were dissolved in double distilled water.

157

158 ***2.5. RNA extraction from intestinal tissue and cDNA preparation***

159 Following dissection and cleaning, intestinal samples (ileum and colon) were stored in
160 RNAprotect Tissue Reagent (Qiagen) at 4˚C until processing. Next, total RNA was isolated
161 using the RNeasy Mini Kit (Qiagen) following the manufacturer's instructions and including a
162 DNase digestion step. Subsequently, cDNA was transcribed using qScript cDNA Synthesis Kit
163 (Quantabio) following the manufacturer's instructions.

164

165 ***2.6. Real-time quantitative PCR (RT-qPCR):***

166 Reactions were prepared with FastStart Sybr Green Master (Merk) following the
167 manufacturer's instructions. In brief, 10 µL reaction mix per well, containing cDNA (20 ng)
168 oligonucleotides (200 nM) and UltraPure distilled water (DNase/RNase free; Invitrogen), were
169 loaded onto 96-well plates. Thermocycling was performed using a StepOnePlus^{TM} Real-Time
170 PCR System (Thermo Fisher). A melt curve was performed at the end of thermocycling to
171 assess the specificity of primers. Single peaks were obtained for all primer pairings.

172 To determine primer efficiency, a standard curve was generated for each pair of primers at
173 cDNA concentrations of 50, 5, 0.5, 0.05 and 0.005 ng/µL and plotting C_t against log
174 concentration. Efficiency was calculated by the following equation: Efficiency = $10^{-(1/slope)}$-1
175 (*27, 28*). Efficiency of reaction values between 90 and 110% were considered acceptable.

176 Gene expression was normalised to the endogenous reference gene *Tbp* for both species.
177 This gene encodes the TATA-binding protein. *Tbp* was chose as it has been proposed as an
178 ideal reference gene for the normalisation of gene expression in intestinal samples of mice
179 and other animals (*29–33*). Relative gene expression was calculated as $2^{-\Delta\Delta Ct}$ (*34*). The primer
180 pairs used are described in Supplementary Table 1.

181

182 ***2.7. Biotinylated hyaluronan binding protein staining*:**

183 Biotinylated hyaluronan binding protein (HABP) staining was performed as previously
184 described (*25*). In brief, 12 µm intestinal tissue sections were washed 3 times in PBS-Tween20
185 and subsequently blocked for 1 hour in a diluent solution (0.2% Triton X-100 and 5% bovine
186 serum albumin in PBS). Slides were then incubated overnight with HABP (Amsbio) in the
187 diluent (1:200) at 4 °C. Next, the slides underwent another round of washing with PBS-
188 Tween20 and were incubated for 2 hours at room temperature with streptavidin conjugated to
189 AlexaFluor 488 (Invitrogen). After three final washes with PBS-Tween20, glass coverslips
190 were mounted onto the slides using MOWIOL mounting medium (Sigma-Aldrich). Samples
191 were imaged using an Olympus BX51 microscope and QImaging camera.

192

193 ***2.8. Measurement of Substance P from intestinal explants***

194 Post-mortem, the small intestine and colon were carefully removed, cleaned of faecal pellets
195 and maintained in ice-cold Krebs solution. Next, 30-50 mg tissue sections (terminal ileum and
196 distal colon) were dissected and transferred into 24-well plates containing 500 µL per well of
197 L-15 Medium (GlutaMAX) medium (Gibco). Explants from both species were incubated for 5
198 min at 32 °C (5% CO_2, 3%O_2). Thereafter, culture supernatant was collected and stored at -
199 80˚C until use. Substance P was measured using an enzyme-linked immunosorbent assay
200 (Substance P ELISA Kit, Cayman Chemicals) according to the manufacturer's instructions.
201 Substance P levels were normalised to protein content upon quantification using the Bradford
202 Assay (Thermo Fisher) following the manufacturer's instructions.

203

204 ***2.9. Statistical analyses:***

205 Tissue was taken from non-manipulated healthy animals being used for other experiments,
206 thus meeting the Reduction aim of the 3Rs. While there were no upfront power calculations to

determine the sample size, we included sample sizes commonly used for the types of assays used in this study (*35, 36*). For histological assessment of mouse and NMR samples, 2-3 per sections per animal, separated by at least 150 µm, were randomly captured, and analysed by an experimenter in a blinded manner. The experimenter was unblinded for statistical analysis.

Normal (Gaussian) distribution was determined for all datasets using the Shapiro–Wilk normality test. Non-parametric tests were used for datasets where ≥1 group did not pass the normality test (assuming $\alpha = 0.05$). Otherwise, parametric tests were used. The type of statistical test and the sample sizes for each experiment are provided in figure legends. Data were plotted and statistical analyses performed with Prism (GraphPad Software version 10.1.1). A *p*-value <0.05 was considered statistically significant. Finally, effect sizes were calculated post hoc using the statistical software G*Power (Version 3.1.9.6).

3. Results:

3.1. Macroscopic features of the naked mole-rat gastrointestinal tract.

Initial evaluation of the gastrointestinal tract gross anatomy showed a noticeably shorter gut length, measured from the pyloric sphincter to the anus, in NMRs compared to mice (mouse 40.09 ± 2.35 cm vs. NMR 22.17 ± 1.94 cm, $p < 0.0001$; Figure 1a, b). Further analyses revealed that these differences were driven by a shorter small intestine in NMR than that of mice (small intestine: mouse 32.69 ± 1.92 cm vs. NMR 14.95 ± 1.88 cm, $p < 0.0001$; colon: mouse 7.40 ± 0.65 cm vs. NMR 7.28 ± 0.59 cm, $p = 0.6425$; Figure 1c, d), in keeping with previous studies (*23, 37*). Of interest, while the ratio of the small intestine/colon length in mice was comparable to that in humans (*38–40*), this was reduced by ~2-fold in NMRs (human 3.956 ± 1.36 vs. mouse 4.52 ± 0.99 vs. NMR 2.07 ± 1.20, $p < 0.0001$; Figure 1d). The lengths of the NMR small intestine and colon were comparable between male and female (small intestine: male 15.50 ± 6.60 cm vs. female 15.05 ± 2.50 cm, $p = 0.5626$; colon: male 7.10 ± 2.00 cm vs. female 7.55 ± 0.20 cm, $p = 0.2265$; Supplementary Figure 1a, b). Given the considerable age range of the NMRs used in our study (minimum age: 23 weeks old; maximum age: 145 weeks old) and their attainment of adulthood at ~1 year old, we analysed the relationship between gut length and both age and weight. The colon length was not associated with the age or weight of the NMR (age vs. length: r = 0.0581, p = 0.8248, weight vs. length: r = 0.0245, p = 0.9339; Supplementary Figure 1c, d). However, we did find statistically significant correlations between the small intestine length and the age and weight of NMRs (age vs. length: r = 0.7293, p = 0.0012, weight vs. length: r = 0.6258, p = 0.0282; Supplementary Figure 1e, f). These findings parallel human anatomical data, that is, the length of the colon in young/adolescent individuals is similar to that in adults (*41*), while the small intestine only reaches its maximum length in adulthood (*42*). Overall, these results show gross anatomical differences in the gut of NMRs compared to humans and mice, especially regarding the short length of the small intestine.

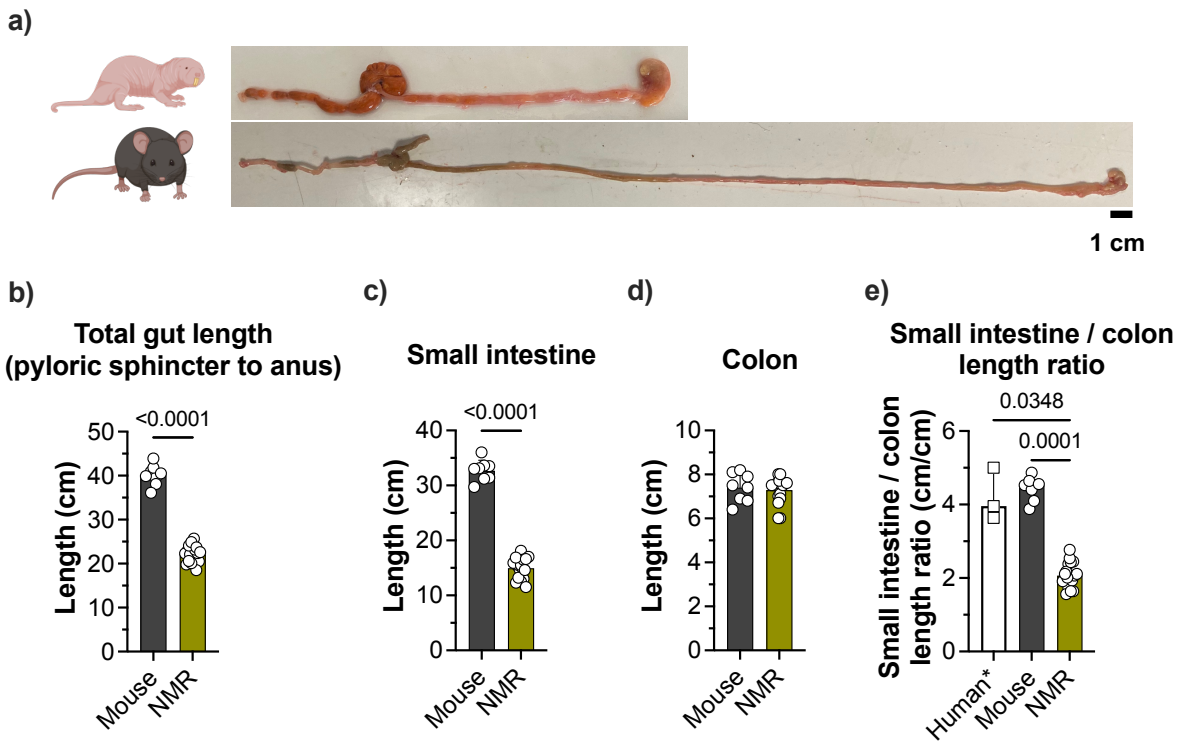

Figure 1. Anatomical features of gastrointestinal tracts of NMRs compared to mice. **a)** Representative pictures of the gastrointestinal tract (from stomach to anus) of NMR (upper panel) and mouse (lower panel). Gastrointestinal length measured from the pyloric sphincter to the anus (**b**), small intestine (**c**) and colon (**d**) in mice (n= 8) and NMRs (n = 17). **e)** Length ratio of the small intestine compared to the colon in humans (data extracted from *(38–40)*), mice and NMR. Human* data reflect median of the means provided by 3 studies that analysed 100, 100 and 200 individuals, respectively. *P* values are shown in plots. **b**, **c** and **d**, unpaired t-test (data shown as mean ± SD); **e**, Kruskal-Wallis test followed by Dunn's multiple comparisons test (data shown as median ± IQR). The NMR and mouse illustrations in **a** were created with BioRender.com).

3.2. Intestinal histology in naked mole-rats

Next, we explored the microscopic architecture of the small intestine (ileum) and colon of NMRs. To this end, we measured the histological properties of the intestinal villi and crypts, as well as the thickness of different layers. The ileum of NMRs showed thicker muscularis (mouse 37.56 ± 8.24 µm vs. NMR 60.45 ± 23.43 µm, $p = 0.0055$; Figure 2a) and submucosal layers compared to mice (mouse 18.90 ± 2.02 µm vs. NMR 40.46 ± 11.22 µm, $p < 0.0001$; Figure 2b). Furthermore, NMR ileal villi were substantially longer (mouse 344.4 ± 180.8 µm vs. NMR 801.0 ± 394.3 µm, $p < 0.0001$; Figure 2c) and wider (mouse 90.95 ± 10.00 µm vs. NMR 135.3 ± 36.63 µm, $p = 0.0008$; Figure 2d) compared to those of mice, and NMR ileal crypts were significantly deeper (mouse -135.60 ± 66.81 µm vs. NMR -157.10 ± 47.49 µm, $p = 0.0039$; Figure 2e) and wider (mouse 35.72 ± 6.45 µm vs. NMR 57.86 ± 10.39 µm, $p < 0.0001$; Figure 2e). In the colon, the muscularis was comparable in both species (mouse 128.2 ± 78.31 µm vs. NMR 139.3 ± 83.82 µm, $p = 0.2188$; Figure 2g), but the colonic submucosa was thicker in NMRs (mouse 63.13 ± 10.18 µm vs. NMR 80.27 ± 10.26 µm, $p = 0.0012$; Figure 2h). Finally, colonic crypts were similarly deep in both species (mouse -219.0 ± 32.57 µm vs. NMR -198.0 ± 12.64 µm, $p = 0.0837$; Figure 2i), but those of NMRs were significantly wider compared to mice (mouse 34.07 ± 3.35 µm vs. NMR 56.79 ± 7.24 µm, $p < 0.0001$; Figure 2j). In summary, these findings indicate that, despite having a shorter small intestine, the ileum of NMRs exhibits features that maximise the surface area for nutrient and water absorption, and ionic

transport, such as ~2.5-fold larger villi compared to mice (Cohen's d size effect = 5.3). Additionally, the larger crypts found in NMRs may be reflective of differences in tissue turnover in these animals compared to mice.

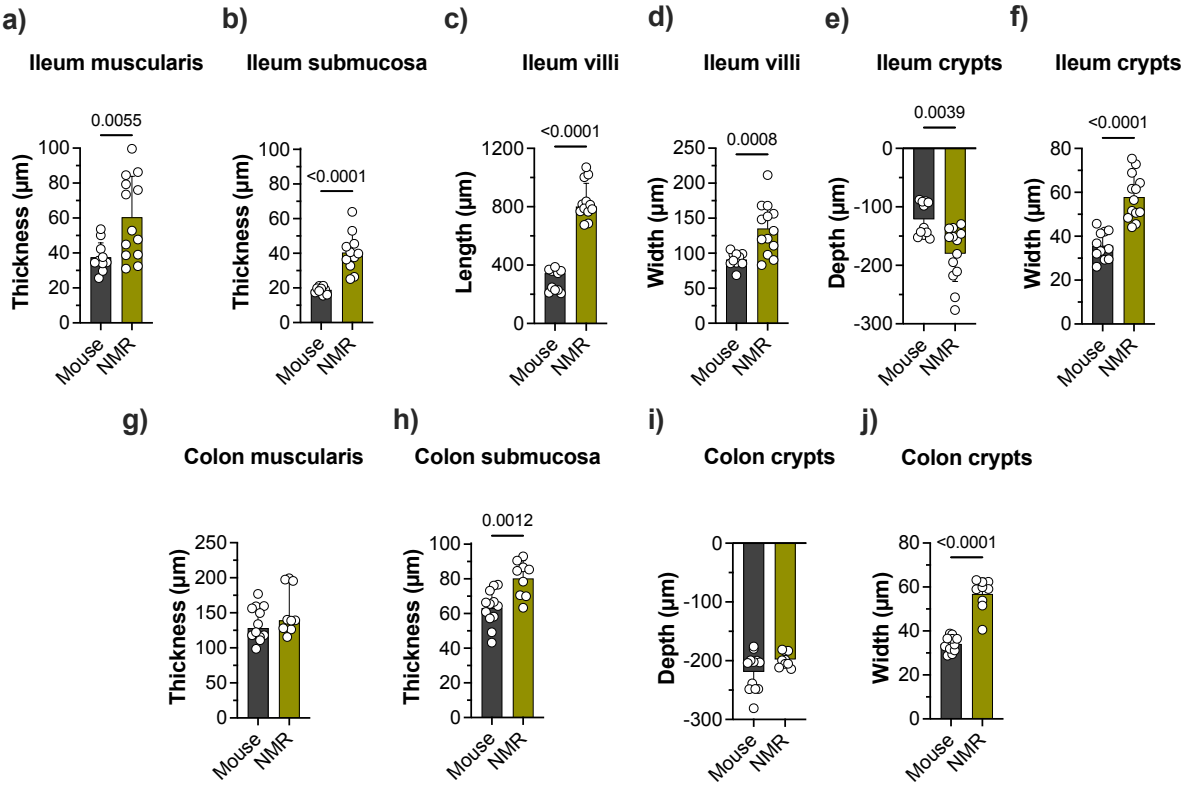

Figure 2. Intestinal histology in NMRs. Ileum muscularis (**a**) and submucosal (**b**) layers thickness in mouse (n = 11) and NMR (n = 13). **c**, average villi height (5-10 villi/sample) in mice (n = 11) and NMRs (n = 12). **d**, average villi width (5-10 villi/sample) in mice (n = 11) and NMRs (n = 13). **e**, average crypt depth (5-10 crypts/sample) in mice (n = 11) and NMRs (n = 13). **f**, average crypt width (5-10 crypts/sample) in mice (n = 11) and NMRs (n = 13). Colon muscularis (**g**) and submucosal (**h**) layers thickness in mouse (n = 12) and NMR (n = 9). **i**, average crypt depth (5-10 crypts/sample) in mice (n = 12) and NMRs (n = 9). **f**, average crypt width (5-10 crypts/sample) in mice (n = 11) and NMRs (n = 13). *P* values are shown in plots. **a**, **b**, **d**, **f**, **h**, **i** and **j**, unpaired t-test (data shown as mean ± SD); **c**, **e** and **g**, Mann-Whitney test (data shown as median ± IQR).

3.3. Intestinal integrity: ileum and colon.

Because of the clear differences in NMR intestinal structures compared to those of mice, we next aimed to examine the physical properties of this tissue. To this end, we used the gold standard technique for this purpose, i.e., the Ussing chamber for measuring mucosal membrane properties. We measured the transepithelial electrical resistance (TEER), as a measure of intestinal barrier integrity. High TEER values are indicative of decreased permeability to ions. Interestingly, the NMR terminal ileum showed a remarkably higher TEER, i.e. reduced permeability, compared to the mouse terminal ileum (mouse 45.41 ± 19.71 Ω · cm^2 vs. NMR 148.6 ± 67.28 Ω · cm^2, p = 0.0012; Cohen's d size effect = 7.15; Figure 3a, b). The NMR distal colon also showed reduced permeability compared to mice, but the difference was less pronounced (mouse 52.35 ± 20.27 Ω · cm^2 vs. NMR 74.53 ± 16.68 Ω · cm^2, p = 0.0012; Cohen's d size effect = 2.59; Figure 3c, d). While the terminal ileum in mice exhibited greater permeability compared to colon (ileum 45.41 ± 19.71 Ω · cm^2 vs. colon 52.35 ± 20.27 Ω · cm^2, p = 0.0197; Cohen's d size effect = 1.24; Supplementary Figure 2a), which aligns with

prior studies in mice (*43*) and is also noted in rats (*44, 45*) and humans (*45, 46*), the terminal ileum of NMRs was extraordinarily less permeable than their distal colon (ileum 148.6 ± 67.28 $\Omega \cdot cm^2$ vs. colon 74.53 ± 16.68 $\Omega \cdot cm^2$, p = 0.0043; Cohen's d size effect = 5.34; Supplementary Figure 2b). Altogether, these results indicate that the integrity of the gastrointestinal tract in NMRs is increased compared to mice, with the NMR small intestine (ileum) showing a strikingly low tissue permeability.

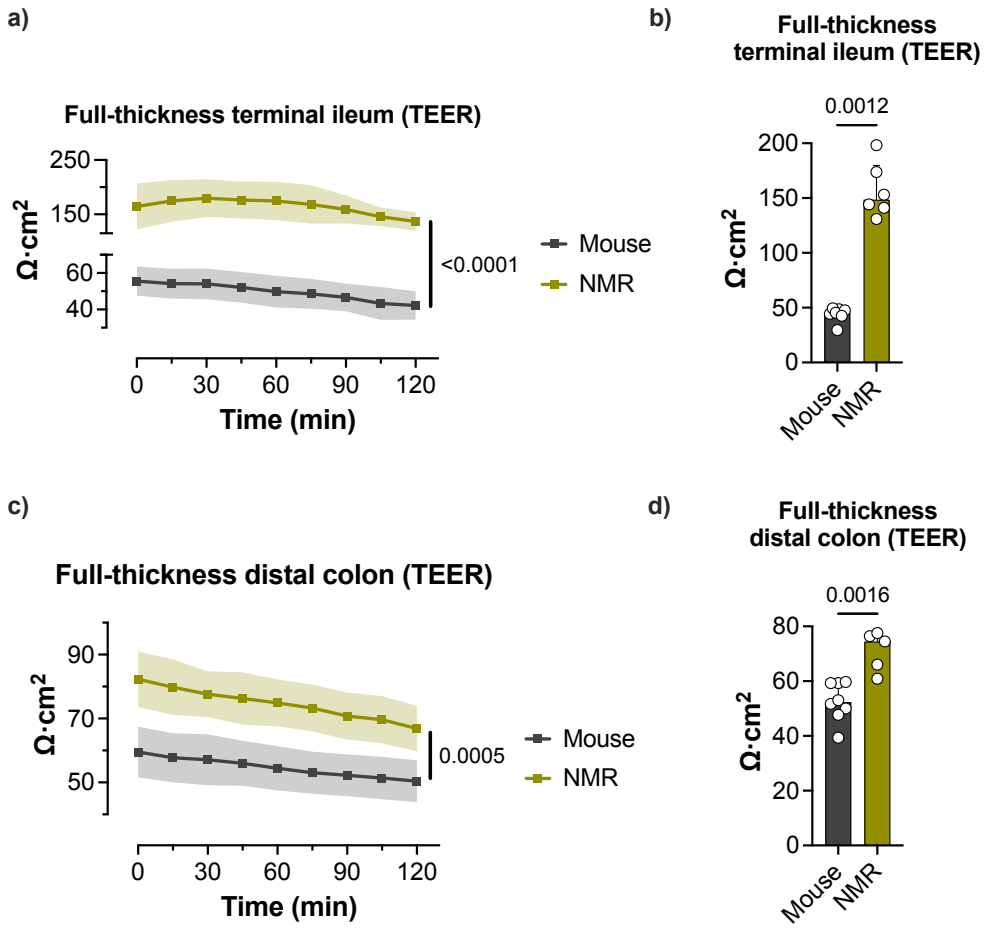

Figure 3. Increased intestinal permeability in NMR. a, b) transepithelial electrical resistance (TEER) in the terminal ileum of mice (n = 7) and NMRs (n = 8). **c, d)** TEER in the distal colon of mice (n = 8) and NMRs (n = 5). Data in **b** and **d** were calculated as the average TEER values between 60 min and 120 min and plotted as individual values. *P* values are shown in plots. **a**, **c**, 2-way ANOVA and Šidak's multiple comparison test (data shown as mean, shadow area represents the SD); **b**, **d**, Mann-Whitney test (data shown as median ± IQR).

3.4. Anion transport in the terminal ileum.

Given the different mucosal integrity properties observed in NMR vs. mouse ileal tissue, we next utilised this region to assess intestinal anion secretion. To this end, we measured the short-circuit current (I_{sc}), as this reflects the net ionic transport, mainly Cl^- and Na^+ in the small intestine, through the mucosa (*6*). An increase in I_{sc} is primarily attributable to anion secretion to the intestinal lumen. We selected four compounds known to evoke anion secretion in rodents and/or humans, such as 5-hydroxytryptamine (5-HT, serotonin) (*47, 48*), bradykinin (*49, 50*), histamine (*51, 52*) and capsaicin (*53, 54*). In keeping with previous studies, we confirmed that 5-HT, bradykinin, histamine and capsaicin evoke a prominent anion secretion to the ileum mucosa in mice (Figure 4a-d). By contrast, ileum preparations from NMRs showed

markedly reduced responses to 5-HT (mouse 179.8 ± 58.15 ΔμA · cm^{-2} vs. NMR 13.23 ± 17.41 ΔμA · cm^{-2}, $p < 0.0001$; Figure 4a) and bradykinin (mouse 78.64 ± 22.04 ΔμA · cm^{-2} vs. NMR 17.98 ± 17.05 ΔμA · cm^{-2}, $p < 0.0001$; Figure 4b), and were virtually unresponsive to histamine (mouse 22.28 ± 24.93 ΔμA · cm^{-2} vs. NMR 3.08 ± 3.16 ΔμA · cm^{-2}, $p = 0.0006$; Figure 4c) and capsaicin (mouse 42.56 ± 20.20 ΔμA · cm^{-2} vs. NMR -0.74 ± 1.98 ΔμA · cm^{-2}, $p = 0.0002$; Figure 4d). These results indicate that NMRs display a pronounced resistance to intestinal ion secretion in response to some neurotransmitters, inflammatory mediators and chemical irritants.

Figure 4. Impaired anion secretion responses in NMRs. a) Short-circuit current increase (ΔI_{sc}) in response to 5-HT in mice (n = 10) and NMRs (n = 11). **b**) ΔI_{sc} in response to bradykinin in mice (n = 10) and NMRs (n = 11). **c**) ΔI_{sc} in response to histamine in mice (n = 7) and NMRs (n = 7). **d**) ΔI_{sc} in response to capsaicin in mice (n = 6) and NMRs (n = 10). For clarity, circles refer to mouse samples and squares to NMRs samples. P values are shown in plots. All data were analysed with Mann-Whitney test (data shown as median ± IQR).

3.5. Expression of receptors involved on intestinal anion transport.

Because NMRs showed impaired anion secretion responses to 5-HT, bradykinin, histamine and capsaicin, we next asked whether NMRs express receptors for these compounds in their intestinal tract. To this end, we used RT-qPCR to evaluate the gene expression of ion channels and receptors associated to these agonists. Importantly, some of these substances can activate several receptors (such as 5-HT, bradykinin and histamine). Hence, we selected genes that encode receptors known to be involved in intestinal anion secretion in humans and/or rodents. Thus, we assessed the gene expression of the 5-HT receptor 4 (*Htr4*) (*47*), the bradykinin receptor B_2 (*Bdkrb2*) (*49*), histamine receptor H_1 (*Hrh1*) (*52*) and the capsaicin receptor transient receptor potential vanilloid 1 (*Trpv1*). Notably, both the terminal ileum and the distal colon of NMR expressed all the genes evaluated. Ileum samples from NMR showed a reduced gene expression of *Bdkrb2* (mouse 0.014 ± 0.039 relative expression vs. NMR 0.001 ± 0.007 relative expression, $p = 0.0002$) and *Hrh1* (mouse 0.11 ± 0.73 relative expression vs. NMR 0.007 ± 0.022 relative expression, $p = 0.0003$) compared to mice, while similar levels of these markers were expressed in the colon of both species (*Bdkrb2*: mouse 0.01 ± 0.02 relative expression vs. NMR 0.01 ± 0.07 relative expression, $p = 0.7984$; *Hrh1*: mouse 0.01 ± 0.008 relative expression vs. NMR 0.01 ± 0.005 relative expression, $p = 0.2220$; Figure 5). On the other hand, colon tissue of NMRs displayed a lower expression of *Htr4* compared to mice (mouse 0.14 ± 0.33 relative expression vs. NMR 0.01 ± 0.03 relative expression, $p = 0.0002$), although no such statistical difference was observed in the ileum across species for *Htr4* (mouse 0.04 ± 0. relative expression vs. NMR 0.18 ± 0.42 relative expression, $p = 0.2785$; Figure 5). These results indicate that, while changes in the gene

expression of these receptors could partially account for the impaired intestinal ion secretion observed in response to some of the compounds evaluated, NMRs express receptors for all these agents along their gastrointestinal tract. Further studies are needed to characterise intestinal secretory responses in these animals.

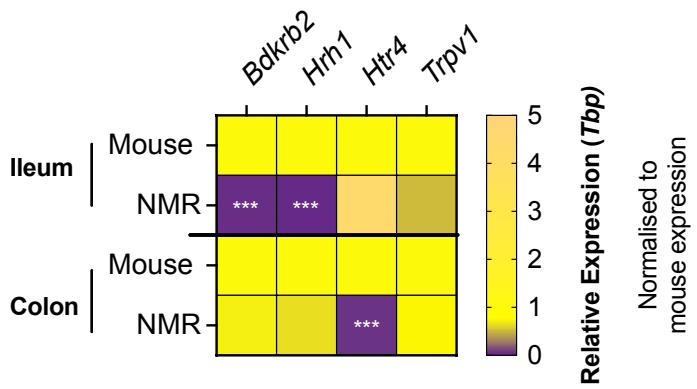

Figure 5. Intestinal gene expression of receptors associated with increased anion secretion. Heatmap of the relative gene expression in terminal ileum and distal colon samples in mice (n = 8) and NMRs (n = 8). All data were analysed with Mann-Whitney test (data shown as colour gradient scale of the relative expression). Each row represents the median of the side-by-side replicates. ***$P < 0.001$.

3.6. Intestinal biomolecules in the gut of naked mole-rats

Finally, we aimed to evaluate biomolecules that have been highlighted to positively contribute to the unusual physiological features found in NMRs. Amongst these, we first focused on hyaluronan, which is an abundant and crucial element in the extracellular matrix of most tissues, including the intestine. This polymer plays a vital role in almost all areas of biology (*55*), including development, tissue architecture, cell proliferation, inflammation, cell migration, etc. Notably, in NMRs, increased levels of hyaluronan can be found in the skin, muscles and lymph nodes (*56, 57*), NMR hyaluronan also displaying a highly folded structure and being able to form gels without the need for chemical crosslinking (*57*). However, hyaluronan levels and localisation in the NMR intestine have not been characterised. To evaluate this, we used specific biotinylated hyaluronan binding protein (HABP) staining. Of note, aside from gross histological dissimilarities discussed above, no marked differences were observed in either the ileum or the colon of NMRs compared to mice (Figure 6a).

Another set of molecules that has garnered considerable interest in NMR is neuropeptides. NMRs do not express substance P and calcitonin gene-related peptide (CGRP) in cutaneous C-fibres and follicles (*58*), in contrast to other mammalian species, including mice. Nevertheless, NMRs do produce both substance P and CGRP in longitudinal lanceolate endings associated with follicle-sinus complexes and body hair follicles (*58*), likely through Aβ-fibres. In keeping with this, we previously observed $GCPR^+$ fibres in myenteric neurons in the colorectum of NMR (*37*). Therefore, we asked whether substance P is also synthetised in the NMR gut. To this end, we collected supernatants from intestinal explants (terminal ileum and distal colon) and analysed the presence of substance P by enzyme immunoassay. The levels of substance P under basal conditions were similar between NMRs and mice (mouse 1.38 ± 2.033 pg substance P · mg $protein^{-1}$ vs. NMR 1.09 ± 1.38 pg substance P · mg $protein^{-1}$, $p > 0.9999$; Figure 6b).

Altogether, these findings indicate that NMRs display a similar hyaluronan localisation along the gut compared to mice, and that basal intestinal levels of substance P are comparable in both species. Further studies will evaluate the distribution of hyaluronan with different molecular weights in the NMR intestine and how this molecule, substance P, and other neuropeptides modulate the gut physiology of these animals.

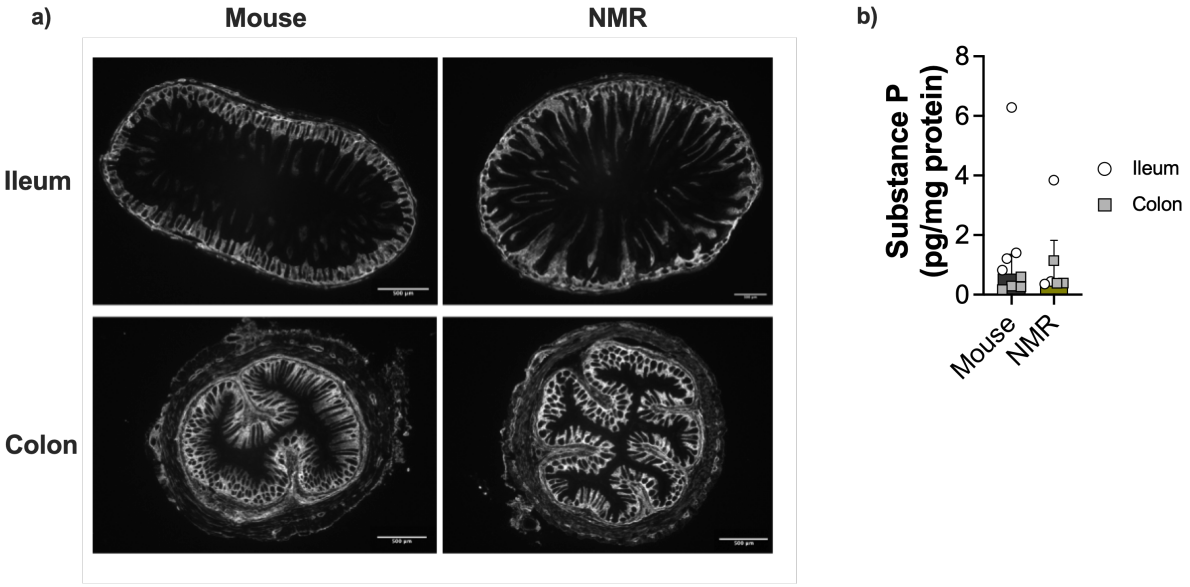

Figure 6. Biomolecules in the gut of NMRs. **a**) Representative images of HABP staining of the terminal ileum of mice (upper left panel) and NMR (upper right panel), and the distal colon of mice (lower left panel) and NMR (lower right panel). Scale bars, 500 µm. **b**) Intestinal levels of substance P (normalised by the content of protein) in mouse (n = 8; 4 ileum samples and 4 colon samples) and NMR (n = 6; 3 ileum samples and 3 colon samples). White circles refer to terminal ileum samples and grey squares to colon samples. **b**, Mann-Whitney test (data shown as median ± IQR).

4. Discussion:

In the present study, we investigated the intestinal barrier function in NMRs as a potential emergent animal model in gastroenterology. Intestinal barrier dysfunction is considered one of the potential underlying pathophysiological mechanisms of many gastrointestinal diseases (*6*), and thus deemed to be of great biological and clinical relevance (*11*). The persisting incidence and prevalence of gastrointestinal conditions in the last decades (*1*) reflects the unmet need for novel strategies in the field. Here, we used NMRs as a non-traditional animal model due to their exceptional biological features (*59*) and studied their physiological intestinal features. We found that the NMR small intestine was significantly shorter compared to that of mice, although it displayed a more robust tissue architecture. In keeping with this, the integrity (measured as TEER by Ussing chambers) of the NMR ileum was remarkably increased compared to the mouse ileum. The colon of NMR, on the other hand, showed more structural similarities to mice, but again displayed superior integrity. The latter can likely be explained by the thicker submucosa found in the colon of NMRs. Of particular interest, we found that the ileum of NMRs showed impaired anion secretion responses to 5-HT, bradykinin, histamine and capsaicin, even though receptors for these agonists were expressed in the gastrointestinal tract. Taken together, NMRs represent a novel animal model of great interest for gastroenterology and, particularly, for studying intestinal barrier function.

428 We first characterised the morphoanatomical features of the intestinal tract in NMRs. The
429 NMR's notably shorter small intestinal length has likely led to the simultaneous development
430 of long villi compared to mice, or rats (*60*). NMRs do not drink water and fulfil their hydration
431 requirements entirely through their solid diet. Therefore, we presume that longer villi enable
432 NMRs to increase the surface area to volume ratio for nutrient and water absorption, which
433 has led to water consumption being redundant. In keeping with this, a recent study showed
434 that long villi are found along the entire small bowel of NMR (*23*), as well as enterocytes
435 involved in the digestion and absorption of nutrients and water (*23, 61*).

436 Notably, the histological features of the NMRs small intestine and colon more closely resemble
437 those of bigger rodents, such as rats (*62*) and guinea pigs (*63, 64*). This is of particular interest
438 because the altered intestinal architecture found in NMRs would not completely explain the
439 increased ileum tissue integrity observed in these animals compared to mice. In fact, previous
440 studies utilising Ussing chambers have reported >2-fold lower TEER values in the ileum of
441 guinea pigs (*65*) and rats (*66, 67*) compared to our results in NMRs, and similar values in the
442 colon of rats (*66–68*) compared to our findings. This strongly suggests that the small intestine
443 of NMRs possesses strong tight junction structures that increase the integrity of this barrier. In
444 the current study, we measured TEER as a proxy for intestinal integrity, which reflects the net
445 flux of anions and cations across the intestinal barrier, including the contribution of the
446 paracellular resistance (resistance of the tight junctions), the transcellular resistance
447 (resistance to ions of the apical and basolateral membranes), and the subepithelial resistance
448 (*6*). Due to the crucial role of tight junctions (i.e., claudin, occludin, zonula occludens-1, and
449 junctional adhesion molecule-A) to selectively regulate the paracellular flux of ions, the
450 regulation of these barrier components is of great relevance. Future studies will assess the
451 expression, organisation and interprotein interactions of tight junctions in the NMR small
452 intestine and how these control the high-capacity pore pathway (permeable to small ions and
453 small uncharged molecules) and the low-capacity leak pathway (permeable to larger
454 macromolecules) in their intestinal barrier (*69*). Overall, the specific characteristics of the NMR
455 small intestine may represent an interesting model for studying intestinal barrier dysfunction
456 in coeliac disease (*70*) and irritable bowel syndrome (*71*), amongst other conditions. Indeed,
457 we note the interesting results from a recent study showing that NMRs displayed no colonic
458 histological damage, even when exposed to 8.75% DSS, albeit for only 3-days (*23*).

459 Another crucial function of the intestinal barrier is the transport of ions and fluids across the
460 epithelium. Disruption of this well-coordinated process may lead to diarrhoea when the gut's
461 capacity for fluid absorption is exceeded. Of note, we found that the NMR ileum displays
462 impaired anion secretion responses to four different compounds: 5-HT, bradykinin, histamine
463 and capsaicin. The bradykinin result aligns with our prior observation that this inflammatory
464 mediator fails to activate colonic afferent nerves in NMRs (*37*). However, we did observe that
465 bradykinin led to mechanical sensitisation of these fibres (*37*), suggesting that they express
466 functional bradykinin receptors B_2. In the present study, we confirmed that NMRs indeed
467 express *Bdkrb2* (gene encoding the bradykinin receptor B_2) in both the colon and ileum.
468 However, differences in the functionality of these receptors and the downstream effector
469 signalling in NMRs remain to be elucidated. Future studies will also explore the different cells
470 expressing this marker (epithelial cells (*72*) and nerve fibres (*73*)) in NMRs, and how these
471 modulate visceral pain and mucosal ion secretion. The role of 5-HT in the NMR gastrointestinal
472 tract has not been previously characterised. While fibroblasts isolated from the back skin or

473 the lungs of NMRs express high levels of 5-HT (*74*), plasma circulating levels of this
474 neurotransmitter are significantly lower compared to mice (*75*). In the gut, we showed that the
475 anion secretion induced by 5-HT was decreased in NMRs compared to mice, although the
476 expression of *Htr4* in the ileum was similar in both species. Further studies are therefore
477 required to determine the functionality of this and other serotonergic receptors, such as 5-HT
478 receptors 1, 2 and 3 (*76*), in different cell types in the NMR intestine. Finally, the lack of
479 cutaneous neuropeptides and unusual connectivity of cutaneous afferent neurons in the spinal
480 cord in NMRs have been proposed to explain the absence capsaicin-induced nocifensive
481 behaviour and associated thermal hypersensitivity (*77*), as well as the lack of histamine-
482 induced scratching behaviour (*78*) in these animals. It should be noted that the lack of
483 substance P and CGRP alone cannot completely explain the lack of nocifensive behaviours
484 induced by these compounds, as substance P and CGRP double knockout mice display intact
485 responses to mechanical, thermal, chemical, visceral pain, itch, and neurogenic inflammation
486 (*79*). In the present study, we showed that despite the virtually complete absence of anion
487 secretion induced by histamine and capsaicin in NMRs, these animals display intestinal basal
488 levels of substance P comparable to mice. Future studies will investigate the role of substance
489 P and other neurotransmitters/neuropeptides in the gut physiology of NMRs, as well as their
490 sources. Overall, we propose that NMRs may be a promising model for the pathogenesis of
491 inflammation-associated diarrhoea in inflammatory bowel disease (*80*) and serotonin- and
492 histamine-associated diarrhoea in irritable bowel syndrome (*81, 82*).

493 It should be highlighted that our study has some limitations. Although physiologically age-
494 matched animals for both species were used, intestinal permeability typically changes
495 throughout the lifetime. However, it should be noted that differences in intestinal permeability
496 between mice and NMRs are in the opposite direction of what one would expect, that is, an
497 increased permeability in older animals (*83*). Interestingly, we found that the ileum permeability
498 was similar in young NMRs compared to older animals (young 153.0 ± 57.09 $\Omega \cdot cm^2$ vs. older
499 144.2 ± 42.75 $\Omega \cdot cm^2$, $p = 0.7000$; Supplementary Figure 2c), thus demonstrating that the
500 differences observed between species are not related to age. Furthermore, all NMRs used in
501 the present study were non-breeders and thus we cannot comment on whether or findings
502 would hold true in sexual mature, breeding animals. Sexual maturity is of relevance to our
503 work because it has been shown, for example, that progesterone decreases gut permeability
504 in humans and Caco-2 cells (*84*) and that oestrogen modulates ion secretion in intestinal
505 epithelial cells (*85*). Most of the NMRs used in our study were males (only 1 female was used
506 in TEER experiments and another 1 in short-circuit current experiments), and thus we are
507 unable to draw firm conclusions with regard to any potential sex differences, but being non-
508 breeder animals, all were sexually immature. However, we do not believe that sex and/or state
509 of sexual maturity are likely responsible for the significant differences observed in the NMR
510 ileum, as the relevant hormones would similarly affect the colon, where we found similar
511 values as previously reported in rats (*66–68*). It should be noted as well that the Ussing
512 chambers experiments were performed at 37˚C, that is, 5-7˚C above the NMRs physiological
513 temperature (*86*). However, an increase in the physiological temperature is typically
514 associated with an increase in mucosal permeability (*87, 88*). It remains to be elucidated
515 whether changes in physiological temperature affect intestinal function in NMRs, although one
516 would normally expect changes in the opposite direction to our findings. Finally, other caveats
517 that must be considered are the differences in diet and microbiota between mice and NMRs,

518 which can affect both the intestinal integrity (*89*) and the anion secretion (*90*). Whether specific
519 gut bacteria found in NMRs (*91*) or compounds of their diet are important to improve intestinal
520 barrier function remain to be elucidated.

521 In conclusion, our work illustrates a remarkably low permeability in the NMR small intestine.
522 Moreover, it reveals that these animals have impaired intestinal anion secretion responses to
523 5-HT, bradykinin, histamine, and capsaicin. Overall, this study adds further evidence to the
524 uncommon biological features exhibited by this species. The NMR gut may therefore offer
525 particular insights into the physiology relevant to gastrointestinal conditions and aid in devising
526 strategies for their treatments. Thus, we strongly support the use of this unconventional animal
527 model in further investigations of intestinal barrier function.

528

529 **5. Acknowledgements:**

530 JA-L and EStJS acknowledge funding from the Medical Research Council (MRC)
531 (MR/W002426/1) and AR was supported by AstraZeneca PhD Studentship (G115018).

532

533 **6. Disclosures:**

534 The authors declare no competing interests.

535

536 **7. Author contribution:**

537 JA-L conceptualised and designed the research study, conducted the experiments (Ussing
538 chamber experiments, gene expression, enzyme immunoassays), acquired and analysed the
539 data and wrote the manuscript. AR conducted the experiments (histology and IHC) and
540 acquired the data. DCB provided experimental support and discussed the data. EStJS
541 provided experimental support, reviewed and discussed the data and revised the manuscript.
542 All authors corrected and approved the final version of the manuscript.

543

544 **8. ORCID iD:**

545 Javier Aguilera-Lizarraga: https://orcid.org/0000-0002-8135-9933.

546 Anne Ritoux: https://orcid.org/0000-0002-5760-6172

547 David C. Bulmer: https://orcid.org/0000-0002-4703-7877

548 Ewan St. J. Smith: https://orcid.org/0000-0002-2699-1979.

549

550 **9. References**:

551 1. Y. Wang, Y. Huang, R. C. Chase, T. Li, D. Ramai, S. Li, X. Huang, S. O. Antwi, A. P.
552 Keaveny, M. Pang, Global Burden of Digestive Diseases: A Systematic Analysis of the
553 Global Burden of Diseases Study, 1990 to 2019. *Gastroenterology* **165**, 773-783.e15
554 (2023).
555 2. T. C. Rose, A. Pennington, C. Kypridemos, T. Chen, M. Subhani, J. Hanefeld, L.
556 Ricciardiello, B. Barr, Analysis of the burden and economic impact of digestive

557 diseases and investigation of research gaps and priorities in the field of digestive
558 health in the European Region—White Book 2: Executive summary. *United European*
559 *Gastroenterol J* **10**, 657–662 (2022).
560 3. V. C. Goodoory, C. E. Ng, C. J. Black, A. C. Ford, Direct healthcare costs of Rome IV or
561 Rome III-defined irritable bowel syndrome in the United Kingdom. *Aliment Pharmacol*
562 *Ther* **56**, 110–120 (2022).
563 4. R. S. Sandler, J. E. Everhart, M. Donowitz, E. Adams, K. Cronin, C. Goodman, E.
564 Gemmen, S. Shah, A. Avdic, R. Rubin, The burden of selected digestive diseases in the
565 United States. *Gastroenterology* **122**, 1500–1511 (2002).
566 5. L. A. Pattison, A. Cloake, S. Chakrabarti, H. Hilton, R. H. Rickman, J. P. Higham, M. Y.
567 Meng, L. W. Paine, L. Qiu, A. Ritoux, D. C. Bulmer, G. Callejo, E. St John Smith, Digging
568 deeper into pain – an ethological behavior assay correlating well-being in mice with
569 human pain experience. *bioRxiv*, doi: 10.1101/2023.08.18.553862 (2024).
570 6. T. Vanuytsel, J. Tack, R. Farre, The Role of Intestinal Permeability in Gastrointestinal
571 Disorders and Current Methods of Evaluation. *Front Nutr* **8**, 717925 (2021).
572 7. H. Majamaa, E. Isolauri, Evaluation of the gut mucosal barrier: Evidence for increased
573 antigen transfer in children with atopic eczema. *J Allergy Clin Immunol* **97**, :985-90
574 (1996).
575 8. A. Benard, P. Desreumeaux, D. Huglo, A. Hoorelbeke, A.-B. Tonnel, B. Wallaert, iD Lille,
576 Increased intestinal permeability in bronchial asthma. *J Allergy Clin Immunol* **97**,
577 1173–1181 (1996).
578 9. A. Fasano, N. P. Visanji, L. W. C. Liu, A. E. Lang, R. F. Pfeiffer, Gastrointestinal
579 dysfunction in Parkinson's disease. Lancet Publishing Group [Preprint] (2015).
580 https://doi.org/10.1016/S1474-4422(15)00007-1.
581 10. M. P. Fink, Leaky gut hypothesis: a historical perspective. [Preprint] (1990).
582 https://doi.org/10.1097/00003246-199005000-00024.
583 11. M. Camilleri, Leaky gut: mechanisms, measurement and clinical implications in
584 humans. BMJ Publishing Group [Preprint] (2019). https://doi.org/10.1136/gutjnl-
585 2019-318427.
586 12. H. Vanheel, M. Vicario, T. Vanuytsel, L. Van Oudenhove, C. Martinez, À. V. Keita, N.
587 Pardon, J. Santos, J. D. Soderholm, J. Tack, R. Farré, Impaired duodenal mucosal
588 integrity and low-grade inflammation in functional dyspepsia. *Gut* **63**, 262–71 (2014).
589 13. A. Fedi, C. Vitale, G. Ponschin, S. Ayehunie, M. Fato, S. Scaglione, In vitro models
590 replicating the human intestinal epithelium for absorption and metabolism studies: A
591 systematic review. *Journal of Controlled Release* **335**, 247–268 (2021).
592 14. J. Fogh, T. Orfeo, J. Tiso, F. E. Sharkey, Establishment of human colon carcinoma lines
593 in nude mice. *Exp Cell Biol* **47**, 136–144 (1979).
594 15. M. González-González, C. Díaz-Zepeda, J. Eyzaguirre-Velásquez, C. González-Arancibia,
595 J. A. Bravo, M. Julio-Pieper, Investigating gut permeability in animal models of disease.
596 Frontiers Media S.A. [Preprint] (2019). https://doi.org/10.3389/fphys.2018.01962.
597 16. J. Foulke-Abel, J. In, J. Yin, N. C. Zachos, O. Kovbasnjuk, M. K. Estes, H. De Jonge, M.
598 Donowitz, Human Enteroids as a Model of Upper Small Intestinal Ion Transport
599 Physiology and Pathophysiology. *Gastroenterology* **150**, 638-649.e8 (2016).
600 17. F. Weiß, D. Holthaus, M. Kraft, C. Klotz, M. Schneemann, J. D. Schulzke, S. M. Krug,
601 Human duodenal organoid-derived monolayers serve as a suitable barrier model for
602 duodenal tissue. *Ann N Y Acad Sci* **1515**, 155–167 (2022).

18. A. J. Barker, U. Koch, G. R. Lewin, S. J. Pyott, *The Extraordinary Biology of the Naked Mole-Rat* (2021)vol. 1319.
19. R. Buffenstein, The Naked Mole-Rat: A New Long-Living Model for Human Aging Research. *J Gerontol A Biol Sci Med Sci* **60**, 1369–77 (2005).
20. K. Oka, M. Yamakawa, Y. Kawamura, N. Kutsukake, K. Miura, The Naked Mole-Rat as a Model for Healthy Aging. *Annu Rev Anim Biosci* **11**, 207–226 (2023).
21. G. Maldonado, G. Hernández, Translational control in the naked mole-rat as a model highly resistant to cancer. [Preprint] (2021). https://doi.org/10.1016/j.bbcan.2020.188455.
22. Y. H. Edrey, D. X. Medina, M. Gaczynska, P. A. Osmulski, S. Oddo, A. Caccamo, R. Buffenstein, Amyloid beta and the longest-lived rodent: the naked mole-rat as a model for natural protection from Alzheimer's disease. *Neurobiol Aging* **34**, 2352–60 (2013).
23. S. Montazid, S. Bandyopadhyay, D. W. Hart, N. Gao, B. Johnson, S. G. Thrumurthy, D. J. Penn, B. Wernisch, M. Bansal, P. M. Altrock, F. Rost, P. Gazinska, P. Ziolkowski, B. H. Hayee, Y. Liu, J. Han, A. Tessitore, J. Koth, W. F. Bodmer, J. E. East, N. C. Bennett, I. Tomlinson, S. Irshad, Adult stem cell activity in naked mole rats for long-term tissue maintenance. *Nat Commun* **14**, 8484 (2023).
24. S. Wirtz, V. Popp, M. Kindermann, K. Gerlach, B. Weigmann, S. Fichtner-Feigl, M. F. Neurath, Chemically induced mouse models of acute and chronic intestinal inflammation. *Nat Protoc* **12**, 1295–1309 (2017).
25. T. S. Taylor, P. Konda, S. S. John, D. C. Bulmer, J. R. F. Hockley, E. S. J. Smith, Galanin suppresses visceral afferent responses to noxious mechanical and inflammatory stimuli. *Physiol Rep* **8**, e14326 (2020).
26. S. U. Mondelaers, S. A. Theofanous, M. V. Florens, E. Perna, J. Aguilera-Lizarraga, G. E. Boeckxstaens, M. M. Wouters, W. M. Mondelaers SU, Theofanous SA, Florens MV, Perna E, Aguilera-Lizarraga J, Boeckxstaens GE, S. U. Mondelaers, S. A. Theofanous, M. V. Florens, E. Perna, J. Aguilera-Lizarraga, G. E. Boeckxstaens, M. M. Wouters, Effect of genetic background and postinfectious stress on visceral sensitivity in Citrobacter rodentium-infected mice. *Neurogastroenterology and Motility* **28**, 647–658 (2016).
27. K. R. Rogers-Broadway, E. Karteris, Amplification efficiency and thermal stability of qPCR instrumentation: Current landscape and future perspectives. *Exp Ther Med* **10**, 1261–1264 (2015).
28. D. Svec, A. Tichopad, V. Novosadova, M. W. Pfaffl, M. Kubista, How good is a PCR efficiency estimate: Recommendations for precise and robust qPCR efficiency assessments. *Biomol Detect Quantif* **3**, 9–16 (2015).
29. N. Eissa, H. Hussein, H. Wang, M. F. Rabbi, C. N. Bernstein, J. E. Ghia, Stability of reference genes for messenger RNA quantification by real-time PCR in mouse dextran sodium sulfate experimental colitis. *PLoS One* **11**, e0156289 (2016).
30. N. Eissa, L. Kermarrec, H. Hussein, C. N. Bernstein, J. E. Ghia, Appropriateness of reference genes for normalizing messenger RNA in mouse 2,4-dinitrobenzene sulfonic acid (DNBS)-induced colitis using quantitative real time PCR. *Sci Rep* **7**, 42427 (2017).
31. F. Wang, J. Wang, D. Liu, Y. Su, Normalizing genes for real-time polymerase chain reaction in epithelial and nonepithelial cells of mouse small intestine. *Anal Biochem* **399**, 211–217 (2010).

32. J. Zhang, Y. Y. Gao, Y. Q. Huang, Q. Fan, X. T. Lu, C. K. Wang, Selection of housekeeping genes for quantitative gene expression analysis in yellow-feathered broilers. *Ital J Anim Sci* **17**, 540–546 (2018).
33. A. B. Nygard, C. B. Jørgensen, S. Cirera, M. Fredholm, Selection of reference genes for gene expression studies in pig tissues using SYBR green qPCR. *BMC Mol Biol* **8** (2007).
34. K. J. Livak, T. D. Schmittgen, Analysis of relative gene expression data using real-time quantitative PCR and the 2(-Delta Delta C(T)) Method. *Methods*, doi: 10.1006/meth.2001.1262 (2001).
35. J. Aguilera-Lizarraga, M. V. Florens, M. F. Viola, P. Jain, L. Decraecker, I. Appeltans, M. Cuende-Estevez, N. Fabre, K. Van Beek, E. Perna, D. Balemans, N. Stakenborg, S. Theofanous, G. Bosmans, S. U. Mondelaers, G. Matteoli, S. Ibiza Martínez, C. Lopez-Lopez, J. Jaramillo-Polanco, K. Talavera, Y. A. Alpizar, T. B. Feyerabend, H. R. Rodewald, R. Farre, F. A. Redegeld, J. Si, J. Raes, C. Breynaert, R. Schrijvers, C. Bosteels, B. N. Lambrecht, S. D. Boyd, R. A. Hoh, D. Cabooter, M. Nelis, P. Augustijns, S. Hendrix, J. Strid, R. Bisschops, D. E. Reed, S. J. Vanner, A. Denadai-Souza, M. M. Wouters, G. E. Boeckxstaens, Local immune response to food antigens drives meal-induced abdominal pain. *Nature* **590**, 151–156 (2021).
36. S. De Schepper, S. Verheijden, J. Aguilera-Lizarraga, M. F. Viola, W. Boesmans, N. Stakenborg, I. Voytyuk, I. Smidt, B. Boeckx, I. Dierckx de Casterlé, V. Baekelandt, E. Dominguez Gonzalez, M. Mack, I. Depoortere, B. De Strooper, B. Sprangers, U. Himmelreich, S. Soenen, M. Guilliams, P. Vanden Berghe, E. Jones, D. Lambrechts, G. Boeckxstaens, Self-Maintaining Gut Macrophages Are Essential for Intestinal Homeostasis. *Cell* **175**, 400-415.e13 (2018).
37. J. R. F. Hockley, K. H. Barker, T. S. Taylor, G. Callejo, Z. M. Husson, D. C. Bulmer, E. S. J. Smith, Acid and inflammatory sensitisation of naked mole-rat colonic afferent nerves. *Mol Pain* **16**, 1744806920903150 (2020).
38. F. Treves, Anatomy of the Intestinal Canal and Peritoneum in Man. *British Medical Journal* **1**, 580–583 (1885).
39. B. M. L. Underhill, Intestinal length in man. *British Medical Journal* **2**, 1243–1246 (1955).
40. G. Hounnou, C. Destrieux, J. Desmé, P. Bertrand, S. Velut, Anatomical study of the length of the human intestine. *Surgical and Radiologic Anatomy* **24**, 290–294 (2002).
41. S. Sadahiro, T. Ohmura, Y. Yamada, T. Saito, Y. Taki, Analysis of length and surface area of each segment of the large intestine according to age, sex and physique. *Surg Radiol Anat* **14**, 251–257 (1992).
42. L. T. Weaver, S. Austin, T. J. Cole, M. Dunn, Small intestinal length: a factor essential for gut adaptation. *Gut* **32**, 1321–1323 (1991).
43. N. Hanning, R. Verboven, J. G. De Man, H. Ceuleers, H. U. De Schepper, A. Smet, B. Y. De Winter, Single-day and multi-day exposure to orogastric gavages does not affect intestinal barrier function in mice. *American Journal of Physiology-Gastrointestinal and Liver Physiology* **324**, G281–G294 (2023).
44. L. Feighery, A. Smyth, S. Keely, A. W. Baird, W. T. O'Connor, J. J. Callanan, D. J. Brayden, Increased intestinal permeability in rats subjected to traumatic frontal lobe percussion brain injury. *Journal of Trauma - Injury, Infection and Critical Care* **64**, 131–137 (2008).
45. P. Nejdfors, M. Ekelund, B. Jeppsson, B. R. Weström, Mucosal in vitro permeability in the intestinal tract of the pig, the rat, and man: Species- and region-related differences. *Scand J Gastroenterol* **35**, 501–507 (2000).

46. Å. Sjöberg, M. Lutz, C. Tannergren, C. Wingolf, A. Borde, A. L. Ungell, Comprehensive study on regional human intestinal permeability and prediction of fraction absorbed of drugs using the Ussing chamber technique. *European Journal of Pharmaceutical Sciences* **48**, 166–180 (2013).
47. M. R. Budhoo, R. P. Harris, J. M. Kellum, 5-Hydroxytryptamine-induced Cl- transport is mediated by 5-HT3 and 5-HT4 receptors in the rat distal colon. *Eur J Pharmacol* **298**, 137–144 (1996).
48. M. R. Budhoo, J. M. Kellum, E. Woltering, S. Ashley, B. Bass, The 5-HT4 receptor mediates 5-hydroxytryptamine-induced rise in short circuit current in the human jejunum in vitro. *Surgery* **116**, 396–400 (1994).
49. A. W. Baird, M. M. Skelly, D. P. O'Donoghue, K. E. Barrett, S. J. Keely, Bradykinin regulates human colonic ion transport in vitro. *Br J Pharmacol* **155**, 558–566 (2008).
50. D. C. Manning, S. H. Snyder, J. F. Kachur, R. J. Miller, M. Field, Bradykinin receptor-mediated chloride secretion in intestinal function. *Nature* **299**, 256–259 (1982).
51. Y. Wang, H. J. Cooke, R. Fertel, H. Su, Histamine augments colonic secretion in guinea pig distal colon. *American journal of physiology* **258**, G432–G439 (1990).
52. G. Schultheiss, B. Hennig, W. Schunack, G. Prinz, M. Diener, Histamine-induced ion secretion across rat distal colon: Involvement of histamine H1 and H2 receptors. *Eur J Pharmacol* **546**, 161–170 (2006).
53. S. Yarrow, J. A. Ferrar, H. M. Cox, The effects of capsaicin upon electrogenic ion transport in rat descending colon. *Naunyn-Schmiedeberg's Arch Pharmacol* **344**, 557–563 (1991).
54. E. Weber, M. Neunlist, M. Schemann, T. Frieling, Neural components of distension-evoked secretory responses in the guinea-pig distal colon. *Journal of Physiology* **536**, 741–751 (2001).
55. S. Garantziotis, R. C. Savani, Hyaluronan biology: A complex balancing act of structure, function, location and context. *Matrix Biology* **78–79**, 1–10 (2019).
56. X. Tian, J. Azpurua, C. Hine, A. Vaidya, M. Myakishev-Rempel, J. Ablaeva, Z. Mao, E. Nevo, V. Gorbunova, A. Seluanov, High-molecular-mass hyaluronan mediates the cancer resistance of the naked mole rat. *Nature* **499**, 346–349 (2013).
57. D. del Marmol, S. Holtze, N. Kichler, A. Sahm, B. Bihin, V. Bourguignon, S. Dogné, K. Szafranski, T. B. Hildebrandt, B. Flamion, Abundance and size of hyaluronan in naked mole-rat tissues and plasma. *Sci Rep* **11**, 7951 (2021).
58. T. J. Park, C. Comer, A. Carol, Y. Lu, H. S. Hong, F. L. Rice, Somatosensory organization and behavior in naked mole-rats: II. Peripheral structures, innervation, and selective lack of neuropeptides associated with thermoregulation and pain. *Journal of Comparative Neurology* **465**, 104–120 (2003).
59. R. Buffenstein, V. Amoroso, B. Andziak, S. Avdieiev, J. Azpurua, A. J. Barker, N. C. Bennett, M. A. Brieño-Enríquez, G. N. Bronner, C. Coen, M. A. Delaney, C. M. Dengler-Crish, Y. H. Edrey, C. G. Faulkes, D. Frankel, G. Friedlander, P. A. Gibney, V. Gorbunova, C. Hine, M. M. Holmes, J. U. M. Jarvis, Y. Kawamura, N. Kutsukake, C. Kenyon, W. T. Khaled, T. Kikusui, J. Kissil, S. Lagestee, J. Larson, A. Lauer, L. A. Lavrenchenko, A. Lee, J. B. Levitt, G. R. Lewin, K. N. Lewis Hardell, T. H. D. Lin, M. J. Mason, D. McCloskey, M. McMahon, K. Miura, K. Mogi, V. Narayan, T. P. O'Connor, K. Okanoya, M. J. O'Riain, T. J. Park, N. J. Place, K. Podshivalova, M. E. Pamenter, S. J. Pyott, J. Reznick, J. G. Ruby, A. B. Salmon, J. Santos-Sacchi, D. K. Sarko, A. Seluanov, A. Shepard, M. Smith, K. B. Storey, X. Tian, E. N. Vice, M. Viltard, A. Watarai, E. Wywial, M. Yamakawa, E. D.

742 Zemlemerova, M. Zions, E. S. J. Smith, The naked truth: a comprehensive clarification
743 and classification of current 'myths' in naked mole-rat biology. *Biological Reviews* **97**,
744 115–140 (2022).
745 60. G. E. Holle, Changes in the structure and regeneration mode of the rat small intestinal
746 mucosa following benzalkonium chloride treatment. *Gastroenterology* **101**, 1264–73
747 (1991).
748 61. N. Miron, V. Cristea, Enterocytes: Active cells in tolerance to food and microbial
749 antigens in the gut. [Preprint] (2012). https://doi.org/10.1111/j.1365-
750 2249.2011.04523.x.
751 62. A. Bosi, D. Banfi, M. Bistoletti, L. M. Catizzone, A. M. Chiaravalli, P. Moretto, E. Moro,
752 E. Karousou, M. Viola, M. C. Giron, F. Crema, C. Rossetti, G. Binelli, A. Passi, D. Vigetti,
753 C. Giaroni, A. Baj, Hyaluronan Regulates Neuronal and Immune Function in the Rat
754 Small Intestine and Colonic Microbiota after Ischemic/Reperfusion Injury. *Cells* **11**,
755 3370 (2022).
756 63. M. Mitjans, R. Ferrer, Morphometric Study of the Guinea Pig Small Intestine during
757 Development. *Microsc Res Tech* **63**, 206–214 (2004).
758 64. J. Zhao, D. Liao, J. Yang, H. Gregersen, Biomechanical remodelling of obstructed
759 guinea pig jejunum. *J Biomech* **43**, 1322–1329 (2010).
760 65. R. Moore, C. Pothoulakis, J. Thomas Lamont, S. Carlson, J. L. Madara, J. L. MADARA C
761 difficile, C. difficile toxin A increases intestinal permeability and induces Cl- secretion.
762 *Am J Physiol* **259**, G165-72 (1990).
763 66. L. Feighery, A. Smyth, S. Keely, A. W. Baird, W. T. O'Connor, J. J. Callanan, D. J. Brayden,
764 Increased intestinal permeability in rats subjected to traumatic frontal lobe percussion
765 brain injury. *Journal of Trauma - Injury, Infection and Critical Care* **64**, 131–137 (2008).
766 67. B. I. Polentarutti, A. L. Peterson, À. K. Sjöberg, E. K. I. Anderberg, L. M. Utter, A. L. B.
767 Ungell, Evaluation of viability of excised rat intestinal segments in the Ussing
768 chamber: Investigation of morphology, electrical parameters, and permeability
769 characteristics. *Pharm Res* **16**, 446–54 (1999).
770 68. A. A. Livanova, A. A. Fedorova, A. V. Zavirsky, I. I. Krivoi, A. G. Markov, Dose- and
771 Segment-Dependent Disturbance of Rat Gut by Ionizing Radiation: Impact of Tight
772 Junction Proteins. *Int J Mol Sci* **24**, 1753 (2023).
773 69. L. Shen, C. R. Weber, D. R. Raleigh, D. Yu, J. R. Turner, Tight junction pore and leak
774 pathways: A dynamic duo. *Annu Rev Physiol* **73**, 289–309 (2011).
775 70. R. M. Van Elburg, J. J. Uil, C. J. J. Mulder, H. S. A. Heymans, Intestinal permeability in
776 patients with coeliac disease and relatives of patients with coeliac disease. *Gut* **34**,
777 354–7 (1993).
778 71. A. M. González-Castro, C. Martínez, E. Salvo-Romero, M. Fortea, C. Pardo-Camacho, T.
779 Pérez-Berezo, C. Alonso-Cotoner, J. Santos, M. Vicario, Mucosal pathobiology and
780 molecular signature of epithelial barrier dysfunction in the small intestine in irritable
781 bowel syndrome. [Preprint] (2017). https://doi.org/10.1111/jgh.13417.
782 72. A. W. Baird, M. M. Skelly, D. P. O'Donoghue, K. E. Barrett, S. J. Keely, Bradykinin
783 regulates human colonic ion transport in vitro. *Br J Pharmacol* **155**, 558–66 (2008).
784 73. J. Yi, Z. Bertels, J. S. Del Rosario, A. J. Widman, R. A. Slivicki, M. Payne, H. M. Susser, B.
785 A. Copits, R. W. Gereau, Bradykinin receptor expression and bradykinin-mediated
786 sensitization of human sensory neurons. *Pain* **165**, 202–215 (2024).
787 74. Y. Kawamura, K. Oka, T. Semba, M. Takamori, Y. Sugiura, R. Yamasaki, Y. Suzuki, T.
788 Chujo, M. Nagase, Y. Oiwa, S. Fujioka, S. Homma, Y. Yamamura, S. Miyawaki, M. Narita,

T. Fukuda, Y. Sakai, T. Ishimoto, K. Tomizawa, M. Suematsu, T. Yamamoto, H. Bono, H. Okano, K. Miura, Cellular senescence induction leads to progressive cell death via the INK4a-RB pathway in naked mole-rats. *EMBO J* **42**, e111133 (2023).

75. K. N. Lewis, N. D. Rubinstein, R. Buffenstein, A window into extreme longevity; the circulating metabolomic signature of the naked mole-rat, a mammal that shows negligible senescence. *Geroscience* **40**, 105–121 (2018).

76. M. B. Hansen, A. B. Witte, The role of serotonin in intestinal luminal sensing and secretion. [Preprint] (2008). https://doi.org/10.1111/j.1748-1716.2008.01870.x.

77. T. J. Park, Y. Lu, R. Jüttner, E. S. J. Smith, J. Hu, A. Brand, C. Wetzel, N. Milenkovic, B. Erdmann, P. A. Heppenstall, C. E. Laurito, S. P. Wilson, G. R. Lewin, Selective inflammatory pain insensitivity in the African naked mole-rat (Heterocephalus glaber). *PLoS Biol* **6**, 0156–0170 (2008).

78. E. S. J. Smith, G. R. C. Blass, G. R. Lewin, T. J. Park, Absence of histamine-induced itch in the African naked mole-rat and “rescue” by Substance P. *Mol Pain* **6**, 29 (2010).

79. D. Iain MacDonald, M. Jayabalan, J. Seaman, A. Chesler, Pain persists in mice lacking both 2 Substance P and CGRPα signaling. *bioRxiv*, doi: 10.1101/2023.11.15.567208 (2023).

80. A. N. Anbazhagan, S. Priyamvada, W. A. Alrefai, P. K. Dudeja, Pathophysiology of IBD associated diarrhea. *Tissue Barriers* **6**, e1463897 (2018).

81. W. D. Chey, J. Kurlander, S. Eswaran, Irritable bowel syndrome: A clinical review. American Medical Association [Preprint] (2015). https://doi.org/10.1001/jama.2015.0954.

82. J. D. Wood, Neuropathophysiology of the Irritable Bowel Syndrome. *J Clin Gastroenterol* **35**, S11-22 (2002).

83. N. Thevaranjan, A. Puchta, C. Schulz, A. Naidoo, J. C. Szamosi, C. P. Verschoor, D. Loukov, L. P. Schenck, J. Jury, K. P. Foley, J. D. Schertzer, M. J. Larché, D. J. Davidson, E. F. Verdú, M. G. Surette, D. M. E. Bowdish, Age-Associated Microbial Dysbiosis Promotes Intestinal Permeability, Systemic Inflammation, and Macrophage Dysfunction. *Cell Host Microbe* **21**, 570 (2018).

84. Z. Zhou, C. Bian, Z. Luo, C. Guille, E. Ogunrinde, J. Wu, M. Zhao, S. Fitting, D. L. Kamen, J. C. Oates, G. Gilkeson, W. Jiang, Progesterone decreases gut permeability through upregulating occludin expression in primary human gut tissues and Caco-2 cells. *Sci Rep* **9**, 8367 (2019).

85. X. Yang, Y. Guo, J. He, F. Zhang, X. Sun, S. Yang, H. Dong, Estrogen and estrogen receptors in the modulation of gastrointestinal epithelial secretion. *Oncotarget* **8**, 97683–97692 (2017).

86. V. M. Kovalzon, O. A. Averina, V. A. Minkov, A. A. Petrin, M. Yu. Vysokikh, Unusual Correlation between Rest–Activity and Body Temperature Rhythms in the Naked Mole Rat (Heterocephalus glaber) as Compared to Five Other Mammalian Species. *J Evol Biochem Physiol* **56**, 451–458 (2020).

87. G. P. Lambert, C. V. Gisolfi, D. J. Berg, P. L. Moseley, L. W. Oberley, K. C. Kregel, Selected contribution: Hyperthermia-induced intestinal permeability and the role of oxidative and nitrosative stress. *J Appl Physiol* **92**, 1750–61 (2002).

88. K. Dokladny, P. L. Moseley, T. Y. Ma, Physiologically relevant increase in temperature causes an increase in intestinal epithelial tight junction permeability. *Am J Physiol Gastrointest Liver Physiol* **290**, G204-12 (2006).

89. O. Inczefi, P. Bacsur, T. Resál, C. Keresztes, T. Molnár, The Influence of Nutrition on Intestinal Permeability and the Microbiome in Health and Disease. [Preprint] (2022). https://doi.org/10.3389/fnut.2022.718710.
90. A. C. Engevik, M. A. Engevik, Exploring the impact of intestinal ion transport on the gut microbiota. *Comput Struct Biotechnol J* **19**, 134–144 (2021).
91. T. Debebe, E. Biagi, M. Soverini, S. Holtze, T. B. Hildebrandt, C. Birkemeyer, D. Wyohannis, A. Lemma, P. Brigidi, V. Savkovic, B. König, M. Candela, G. Birkenmeier, Unraveling the gut microbiome of the long-lived naked mole-rat. *Sci Rep* **7**, 9590 (2017).

10. Supplementary information:

Supplementary Table 1. Primer sequences for gene detection by RT-qPCR.

Species	Sequence (5' → 3')	Target marker	NCBI Ref Seq
Mouse	CACCCCCTTGTACCCTTCAC	TATA-box binding protein (*Tbp*)	NM_013684.3
	CAGTTGTCCGTGGCTCTCTT		NM_013684.3
Mouse	CCGGCTCGCTTGAGAAAAGG	Bradykinin receptor β2 (*Bdkrb2*)	NM_009747.2
	CCGACAGAAACCCGAGTAGC		NM_009747.2
Mouse	ACGAGTGAAACCCGATGCTT	Histamine receptor H1 (*Hrh1*)	NM_001252642.3
	CTCTGGCTGTCCTAGGGAGT		NM_001252642.3
Mouse	CCTCACAGCAACTTCTCCTT	5-hydroxytryptamine (serotonin) receptor 4 (*Htr4*)	NM_008313.4
	TCCCCTGACTTCCTCAAATA		NM_008313.4
Mouse	GAGTATGCCCAGAGCCCATC	Transient receptor potential vanilloid 1 (*Trpv1*)	NM_001001445.2
	CAGGCTGCTGTGTGGTAAGA		NM_001001445.2
NMR	TTAATTTCGTTTCCGCGGGC	TATA-box binding protein (*Tbp*)	XM_004868859.3
	GCATAAGGTGGGAGGCTGTT		XM_004868859.3
NMR	CTGGGAGGGAGCTGTAGTCA	Bradykinin receptor β2 (*Bdkrb2*)	XM_021244763.1
	CCTCCTAGGCACTTCCTCCT		XM_021244763.1
NMR	CCCACACGTGGCTTAGAGTT	Histamine receptor H1 (*Hrh1*)	XM_004874845.3
	TTGCTTTGAACATGCAGCCC		XM_004874845.3
NMR	ATGTGGCTCACCACCTTAGC	5-hydroxytryptamine (serotonin) receptor 4 (*Htr4*)	XM_021266180.1
	GTGCCTCATGCCTCACTGAT		XM_021266180.1
NMR	TGTGCAATCGCTGTTCATGC	Transient receptor potential vanilloid 1 (*Trpv1*)	NM_001279859.1
	TGGAAGCCTCGGGTGTAGTA		NM_001279859.1

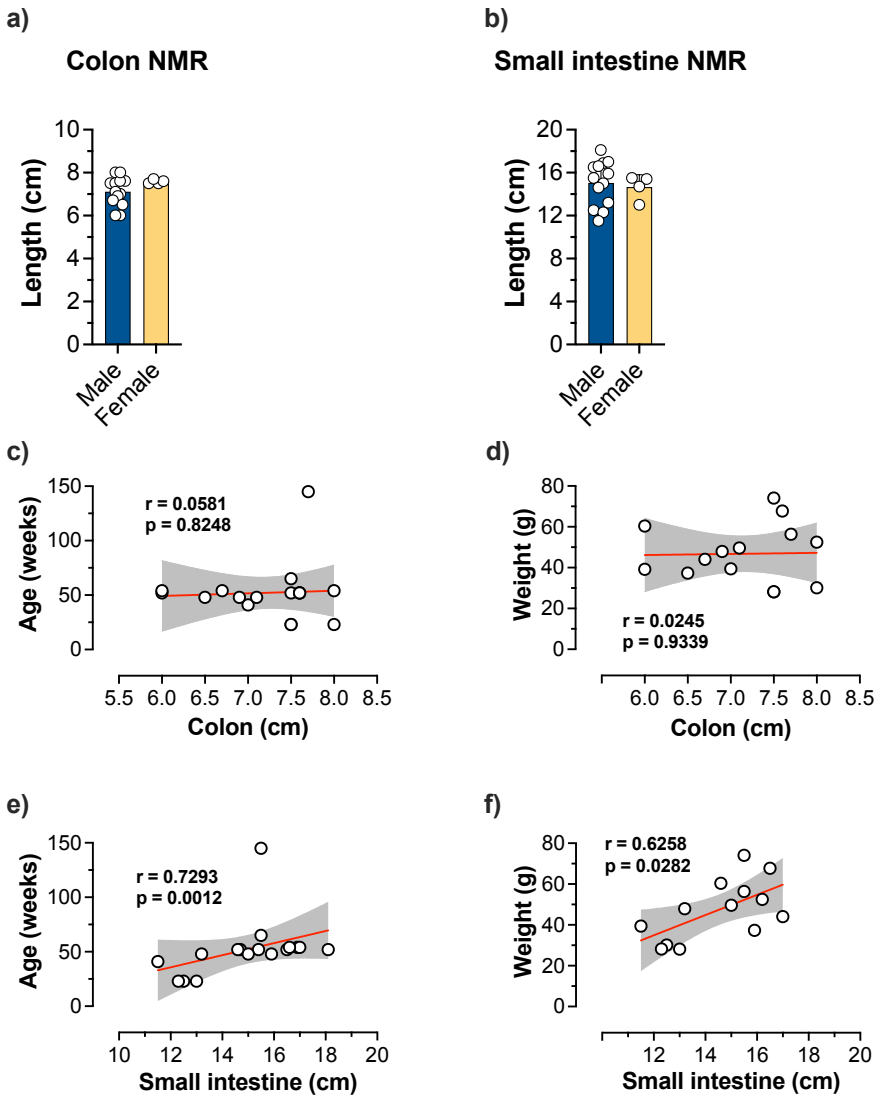

Supplementary Figure 1. Extended anatomical analyses of the NMR gastrointestinal tract. **a)** Colon length in male (n = 13) and female (n = 4) NMRs. **b)** Small intestine length in male (n = 13) and female (n = 4) NMRs. **c)** Correlation between age and colon length in NMRs (n = 17). **d)** Correlation between weight and colon length in NMRs (n = 17). **e)** Correlation between age and small intestine length in NMRs (n = 17). **d)** Correlation between weight and small intestine length in NMRs (n = 16). *P* values are shown in plots. **a** and **b**, Mann Whitney test (data shown as median ± IQR); **c**, **d**, **e** and **f**, two-tailed Pearson's correlation (data shown as individual data, and 95% CI).

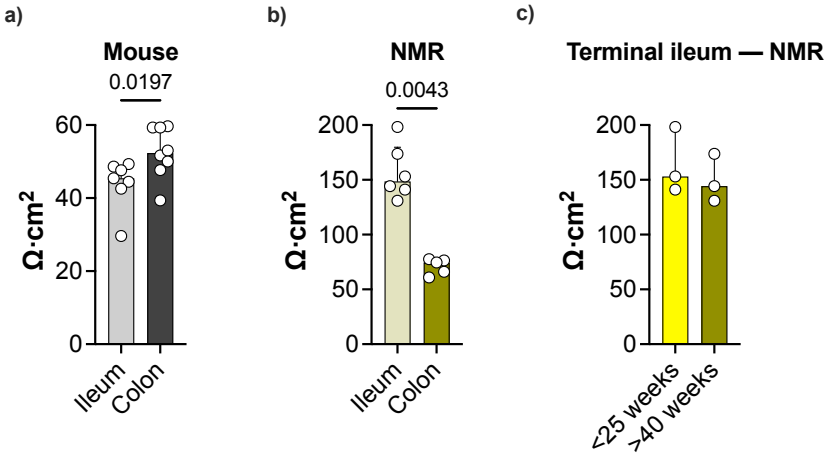

858

859 **Supplementary Figure 2. Extended analyses of the tissue integrity in NMR and mice**. **a)** TEER in the terminal
860 ileum (n = 7) and colon (n = 8) in mice. **b)** TEER in the terminal ileum (n = 6) and colon (n = 5) in NMRs. **c)** TEER
861 in the terminal ileum of young (<25 weeks old; n = 3) and old (>40 weeks old; n = 3) NMRs. Data were calculated
862 as the average TEER values between 60 min and 120 min and plotted as individual values. *P* values are shown in
863 plots. **a**, **b** and **c**, Mann-Whitney test (data shown as median ± IQR).